

# $\gamma$ -ray linear polarization measurements and $(g_{9/2})^{-3}$ neutron alignment in $^{91}\text{Ru}$

Y. Zheng<sup>1,2,\*</sup>, G. de France<sup>1</sup>, E. Clément<sup>1</sup>, A. Dijon<sup>1</sup>, B. Cederwall<sup>3</sup>, R. Wadsworth<sup>4</sup>, T. Bäck<sup>3</sup>, F. Ghazi Moradi<sup>3</sup>, G. Jaworski<sup>5,6</sup>, B.M. Nyakó<sup>7</sup>, J. Nyberg<sup>8</sup>, M. Palacz<sup>6</sup>, H. Al-Azri<sup>4</sup>, G. de Angelis<sup>9</sup>, A. Atac<sup>3,10</sup>, Ö. Aktas<sup>11</sup>, S. Bhattacharyya<sup>1</sup>, T. Brock<sup>4</sup>, P.J. Davies<sup>4</sup>, A. Di Nitto<sup>12,20</sup>, Zs. Dombradi<sup>7</sup>, A. Gadea<sup>13</sup>, J. Gal<sup>7</sup>, P. Joshi<sup>4</sup>, K. Juhasz<sup>14</sup>, R. Julin<sup>15</sup>, A. Jungclaus<sup>16</sup>, G. Kalinka<sup>7</sup>, J. Kownacki<sup>6</sup>, G. La Rana<sup>12</sup>, S.M. Lenzi<sup>17</sup>, J. Molnar<sup>7</sup>, R. Moro<sup>12</sup>, D.R. Napoli<sup>9</sup>, B.S. Nara Singh<sup>4</sup>, A. Persson<sup>3</sup>, F. Recchia<sup>17</sup>, M. Sandzelius<sup>3</sup>, J.-N. Scheurer<sup>18</sup>, G. Sletten<sup>19</sup>, D. Sohler<sup>7</sup>, P.-A. Söderström<sup>8</sup>, M.J. Taylor<sup>4,21</sup>, J. Timar<sup>7</sup>, J.J. Valiente-Dobon<sup>9</sup>, and E. Vardaci<sup>12</sup>

<sup>1</sup> *Grand Accélérateur National d'Ions Lourds (GANIL),*

*CEA/DSM - CNRS/IN2P3,*

*Bd Henri Becquerel, BP 55027,*

*F-14076 Caen Cedex 5, France.*

<sup>2</sup> *Institute of Modern Physics,*

*Chinese Academy of Sciences, Lanzhou, China*

<sup>3</sup> *Department of Physics, Royal Institute of Technology,*

*SE-1069 Stockholm, Sweden.*

<sup>4</sup> *Department of Physics, University of York,*

*YO10 5DD York, UK*

<sup>5</sup> *Faculty of Physics,*

*Warsaw University of Technology,*

*Koszykowa 75, 00-662, Warsaw, Poland.*

<sup>6</sup> *Heavy Ion Laboratory, University of Warsaw,*

*ul. Pasteura 5a, 02-093, Warsaw, Poland.*

<sup>7</sup> *MTA ATOMKI, H-4001 Debrecen, Hungary.*

<sup>8</sup> *Department of Physics and Astronomy,*

*Uppsala University, SE-75120 Uppsala, Sweden.*

<sup>9</sup> *Instituto Nazionale di Fisica Nucleare,*

*Laboratori Nazionali di Legnaro, I-35020 Legnaro, Italy.*

<sup>10</sup> *Department of Physics, Ankara University,*

*06100 Tandogan Ankara, Turkey.*

<sup>11</sup> *Physics Department, Middle East Technical University, 06531 Ankara, Turkey.*

<sup>12</sup> *Dipartimento di Fisica, Università di Napoli and Istituto Nazionale di Fisica Nucleare, I-80126 Napoli, Italy.*

<sup>13</sup> *IFIC, CSIC, University of Valencia, Valencia, Spain.*

<sup>14</sup> *Department of Information Technology,*

*University of Debrecen, H-4010 Debrecen, Hungary.*

<sup>15</sup> *Department of Physics, University of Jyväskylä,*

*FIN-4001 Jyväskylä, Finland.*

<sup>16</sup> *Instituto de Estructura de la Materia,*

*CSIC, E-28006 Madrid, Spain.*

<sup>17</sup> *Dipartimento di Fisica dell'Università di Padova and Istituto Nazionale di Fisica Nucleare,*

*Sezione di Padova, I-35126 Padova, Italy.*

<sup>18</sup> *Université Bordeaux 1, CNRS/IN2P3,*

*Centre d'Etudes Nucléaires de Bordeaux Gradignan,*

*UMR 5797, Chemin du Solarium,  
BP120, 3317 Gradignan, France.*

<sup>19</sup> *The Niels Bohr Institute,  
University of Copenhagen, 2100 Copenhagen, Denmark.*

<sup>20</sup> *Institut für Kernchemie,  
Johannes Gutenberg-Universität Mainz,  
Fritz Strassmann Weg 2, D-55128 Mainz, Germany.*

<sup>21</sup> *School of Physics and Astronomy,  
The University of Manchester,  
Manchester M13 9PL, UK.*

(Dated: November 9, 2018)

Linear polarization measurements have been performed for  $\gamma$ -rays in  $^{91}\text{Ru}$  produced with the  $^{58}\text{Ni}(^{36}\text{Ar}, 2p1n\gamma)^{91}\text{Ru}$  reaction at a beam energy of 111 MeV. The EXOGAM Ge clover array has been used to measure the  $\gamma$ - $\gamma$  coincidences,  $\gamma$ -ray linear polarization and  $\gamma$ -ray angular distributions. The polarization sensitivity of the EXOGAM clover detectors acting as Compton polarimeters has been determined in the energy range 0.3–1.3 MeV. Several transitions have been observed for the first time. Measurements of linear polarization and angular distribution have led to the firm assignments of spin differences and parity of high-spin states in  $^{91}\text{Ru}$ . More specifically, calculations using a semi-empirical shell model were performed to understand the structures of the first and second ( $21/2^+$ ) and ( $17/2^+$ ) levels. The results are in good agreement with the experimental data, supporting the interpretation of the non yrast ( $21/2^+$ ) and ( $17/2^+$ ) states in terms of the  $J_{\text{max}}$  and  $J_{\text{max}} - 2$  members of the seniority-three  $\nu(g_{9/2})^{-3}$  multiplet.

PACS numbers: 23.20.Lv,23.20.En,25.70.Gh,27.60.+j

---

\* zhengyong@impcas.ac.cn

## I. INTRODUCTION

The  $Z > 40$   $N = 47$  nuclei are three neutron holes below the  $N = 50$  closed shell. Their low-lying positive-parity level structure can be interpreted in terms of the spherical shell model as an interplay between proton-particle and neutron-hole excitations in the  $g_{9/2}$  orbital. The possible excitations would then be those belonging to the seniority-three configurations:  $\nu(g_{9/2})^{-3}$ , which can generate spins up to  $21/2^+$  and  $\pi(g_{9/2})^2\nu(g_{9/2})^{-1}$ , terminating at spin  $25/2^+$ . The results of g-factor measurements for the lowest  $8^+$  state in the  $N = 48$  isotones  $^{86}\text{Sr}$  [1],  $^{88}\text{Zr}$  and  $^{90}\text{Mo}$  [2] indicate that it is essentially built from the alignment of a  $g_{9/2}$  neutron pair with a small proton admixture which increases with  $Z$ . Therefore, the neutron aligned  $\nu(g_{9/2})_{J^\pi=21/2^+}^{-3}$  state would be expected to be yrast in the level structure of  $N = 47$  isotones.

The high-spin level structure of  $^{89}\text{Mo}$  ( $Z = 42$ ,  $N = 47$ ) has been studied by M. Weiszflog et al. [3]. The Shell Model interpretation performed with the code RITSSCHIL [4] and within the  $(p_{1/2}, g_{9/2})$  model space indicates that the positive-parity states up to  $25/2^+$  mainly consist of the proton aligned  $\pi(g_{9/2})^2\nu(g_{9/2})^{-1}$  configuration. A particularly interesting case is the one of the  $21/2^+$  state. This state can be generated in the neutron fully aligned  $\nu(g_{9/2})^{-3}$  configuration but the calculations indicate that this component is as small as 1%. This interpretation has been confirmed by g-factor measurements of the  $21/2^+$  isomeric state in  $^{89}\text{Mo}$ , proving the dominance of the  $g_{9/2}$  proton alignment [5].

The trend observed in the  $N = 48$  isotones and the measurement in  $^{89}\text{Mo}$  indicate an evolution from neutron to proton alignment, to generate high-spin states in this mass region. In particular the  $21/2^+$  states in the  $N = 47$  isotope  $^{91}\text{Ru}$  might reveal a complex structure. Understanding the microscopic structure of these levels should therefore shed light on the competition between the possible seniority schemes for the active  $g_{9/2}$  protons and neutrons.

Several groups have already studied the high-spin level structure of  $^{91}\text{Ru}$  [6–9]. Measurements using  $\beta$ -decay,  $\gamma$ - $\gamma$  and  $n$ - $\gamma$  coincidences as well as  $\gamma$ -ray anisotropy ratios have been performed and a level scheme proposed. However, all the spin and parity assignments were based on indirect evidences, systematics or Directional Correlations of the  $\gamma$ -rays deexciting Oriented states (DCO ratios) with fairly large uncertainties and had to be considered as very tentative. The proper way to firmly assign a parity to an excited state is to determine the electromagnetic character of the transition deexciting this particular state. To do this, it is necessary to measure its linear polarization. When combining the polarization information with the angular distribution measurements, the spins and parities of the excited states can be reliably determined. In recent years, due to its high polarization sensitivity and detection efficiency the Ge clover detector [10, 11] has become a useful tool for the measurement of linear polarization by using Compton scattering between adjacent crystals.

In the present work we report on the results of linear polarization measurements in  $^{91}\text{Ru}$  populated in the fusion-evaporation reaction  $^{58}\text{Ni}(^{36}\text{Ar}, 2p1n)^{91}\text{Ru}$  by using the EXOGAM Ge clover detector array [12]. As a result of this work, non yrast ( $21/2^+$ ) and ( $17/2^+$ ) states have been observed for the first time and added to the positive-parity structure of  $^{91}\text{Ru}$ . A theoretical understanding of the structures of the first and second ( $21/2^+$ ) and ( $17/2^+$ ) levels has been obtained in terms of semi-empirical shell model calculations. In addition, the polarization sensitivity of the EXOGAM clover detectors, acting as Compton polarimeters, have been determined over a wide range of  $\gamma$ -ray energies for the first time.

The paper is organized as follows: a description of the experiment at GANIL and the data analysis with a special

emphasis on the polarization measurements and the first characterization of EXOGAM as a Compton polarimeter will be presented in section II. In section III, we present the results obtained for  $^{91}\text{Ru}$  while the Shell Model calculations we performed to understand the microscopic nature of the high-spin states in this nucleus will be discussed in section IV.

## II. EXPERIMENT AND DATA ANALYSIS

Excited states in  $^{91}\text{Ru}$  have been investigated using the fusion-evaporation reaction  $^{58}\text{Ni}(^{36}\text{Ar}, 2p1n)$  at a beam energy of 111 MeV and with an average intensity of 10 pA. The beam was provided by the CIME cyclotron of GANIL, Caen, France. The isotopically enriched (99.83%)  $^{58}\text{Ni}$  targets used in the reactions had an average thickness of  $6.0 \text{ mg/cm}^2$ , enough to stop the recoiling nuclei. The  $\gamma$ -rays from the reaction products were detected by the EXOGAM Ge clover detector array [12], consisting of 11 clover-type Ge detectors for this experiment, 7 at an angle of  $90^\circ$  and 4 at  $135^\circ$  relative to the beam direction. Neutrons evaporated from the compound nuclei were detected using the Neutron Wall array [13] composed of 50 organic liquid-scintillator elements, covering the forward  $1\pi$  section of the solid angle around the target position. The light charged particles (mainly protons and alphas) were detected by the DIAMANT detector system consisting of 80 CsI scintillators [14, 15]. Details of the experiment have been described earlier [16]. Events were collected when at least one neutron was detected by the Neutron Wall and one  $\gamma$ -ray registered in coincidence in the clover detectors. With these trigger conditions a total of  $4 \times 10^9$  events were recorded.

In the off-line processing, coincidence data were sorted into symmetric  $\gamma$ - $\gamma$  matrices with different conditions on the number of detected neutrons and charged particles. These conditions were used to assign new  $\gamma$ -rays to  $^{91}\text{Ru}$ . Coincidence  $\gamma$ -ray spectra were then obtained by setting gates in these matrices.

Examples of coincidence spectra are shown in Fig. 1. Fig. 1(a) is the total projection of a  $\gamma$ - $\gamma$  matrix obtained in coincidence with the detection of two protons and one neutron. This spectrum is dominated by  $\gamma$ -rays from  $^{91}\text{Ru}$  with some peaks belonging to  $^{49}\text{Cr}$  produced in the  $^{16}\text{O}(^{36}\text{Ar}, 2p1n)$  reaction, i.e. in the same reaction channel. This contamination is removed by setting an additional selection of known  $\gamma$ -rays in  $^{91}\text{Ru}$ . Fig. 1(b) shows the spectrum obtained after gating on the 974 keV transition previously known as deexciting the first excited state to the ground state in  $^{91}\text{Ru}$ . This spectrum contains only known transitions belonging to  $^{91}\text{Ru}$  with some additional, unknown  $\gamma$ -rays. Further gating on these new transitions has allowed us to confirm their assignment to  $^{91}\text{Ru}$  and to position them into the level scheme. This is what is shown in Fig. 1(c) which gives a spectrum gated on the new 436 keV transition of  $^{91}\text{Ru}$ . Finally, with the large statistics obtained during this experiment it is possible to perform a more detailed analysis of the observed transitions. The geometry of the EXOGAM array allowed the assignments of spins from the information on DCO ratios [17]. For this purpose, an asymmetric particle-gated matrix was constructed in which  $\gamma$  events recorded at  $90^\circ$  were sorted against those recorded at  $135^\circ$ . The experimental DCO ratios ( $R_{\text{DCO}}$ ) were deduced from pairs of gated spectra according to equation

$$R_{\text{DCO}} = \frac{I(\gamma_1 \text{ at } 135^\circ; \text{ gated by } \gamma_2 \text{ at } 90^\circ)}{I(\gamma_1 \text{ at } 90^\circ; \text{ gated by } \gamma_2 \text{ at } 135^\circ)}. \quad (1)$$

The detection efficiencies of detectors at  $90^\circ$  and at  $135^\circ$  have the same behaviour with  $\gamma$ -ray energy. Therefore their ratio  $R_{\text{eff}}$  is a constant ( $R_{\text{eff}} = 1.79 \pm 0.05$ ) hence no efficiency correction of the DCO ratios was needed. Fig. 2 shows

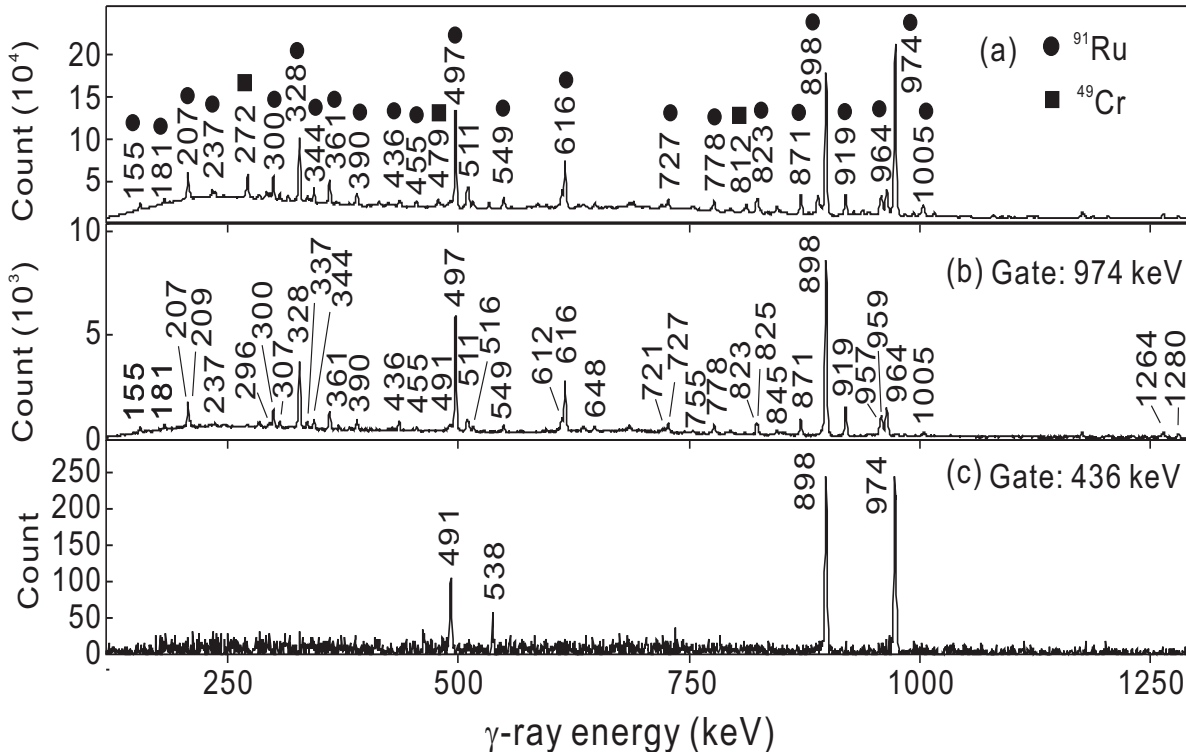


FIG. 1. (a) The total projection of a  $\gamma$ - $\gamma$  matrix obtained in coincidence with two protons and one neutron; the  $\gamma$ -ray peaks are transitions in  $^{91}\text{Ru}$  and  $^{49}\text{Cr}$ . (b) A background subtracted spectrum of  $\gamma$ -rays in coincidence with the 974 keV  $\gamma$ -ray, corresponding to the transition that depopulates the  $(13/2^+)$  state in  $^{91}\text{Ru}$ . (c) A spectrum gated on the 436 keV transition of  $^{91}\text{Ru}$  observed by the present work.

two projected spectra obtained from the DCO matrix. The spectrum in the upper (lower) panel corresponds to  $\gamma$ -rays detected at  $135^\circ$  ( $90^\circ$ ) and in coincidence with the 497 keV  $(21/2^+) \rightarrow (17/2^+)$  transition in  $^{91}\text{Ru}$  observed at  $90^\circ$  ( $135^\circ$ ). The ratio of the peak intensities in these two spectra provides the  $R_{\text{DCO}}$  values of the  $\gamma$ -rays. For example, the three most intense transitions in both projected spectra shown in Fig. 2 are the 616, 898 and 974 keV  $\gamma$ -rays. Their intensities in the two spectra are [2414(62), 6879(90), 6731(88)] and [4821(80), 7134(92), 7062(90)], respectively. The deduced DCO ratios for these transitions are then [0.50(2), 0.96(2), 0.95(2)]. The DCO ratios measured for  $\gamma$ -rays in  $^{91}\text{Ru}$  and also in  $^{91}\text{Tc}$  produced in the  $3p$  channel are shown in Fig. 3. The  $R_{\text{DCO}}$  value for known stretched quadrupole transitions is  $\sim 1$  and is  $\sim 0.6$  for known pure stretched dipoles, when gating on quadrupole transitions. If the gate is set on a pure stretched dipole transition, then the  $R_{\text{DCO}}$  value for known quadrupole transitions is  $\sim 1.6$  and is  $\sim 1$  for known pure stretched dipoles. Based on these assignment criteria, the  $R_{\text{DCO}}$  values obtained in the above example suggest that the 616 keV transition is a  $\Delta I = 1$  dipole transition whereas the 898 and 974 keV transitions have a  $\Delta I = 2$  quadrupole character. These assignments are consistent with the previous assignments [6, 7]. It should be noted that for mixed  $M1 + E2$  transitions  $R_{\text{DCO}}$  ratios can vary between 0.6 and 1.0 depending on the  $\delta$  multipole mixing ratio of the  $\gamma$ -ray. A further ambiguity arises for non-stretched ( $\Delta I = 0$ ) pure  $E1$  (or  $M1$ ) transitions, where  $R_{\text{DCO}}$  for non-stretched dipole transition with  $\delta \approx 0$  mixing ratio is approximately the same as for a stretched quadrupole transition [18, 19]. These ambiguities can be resolved by simultaneously measuring the linear

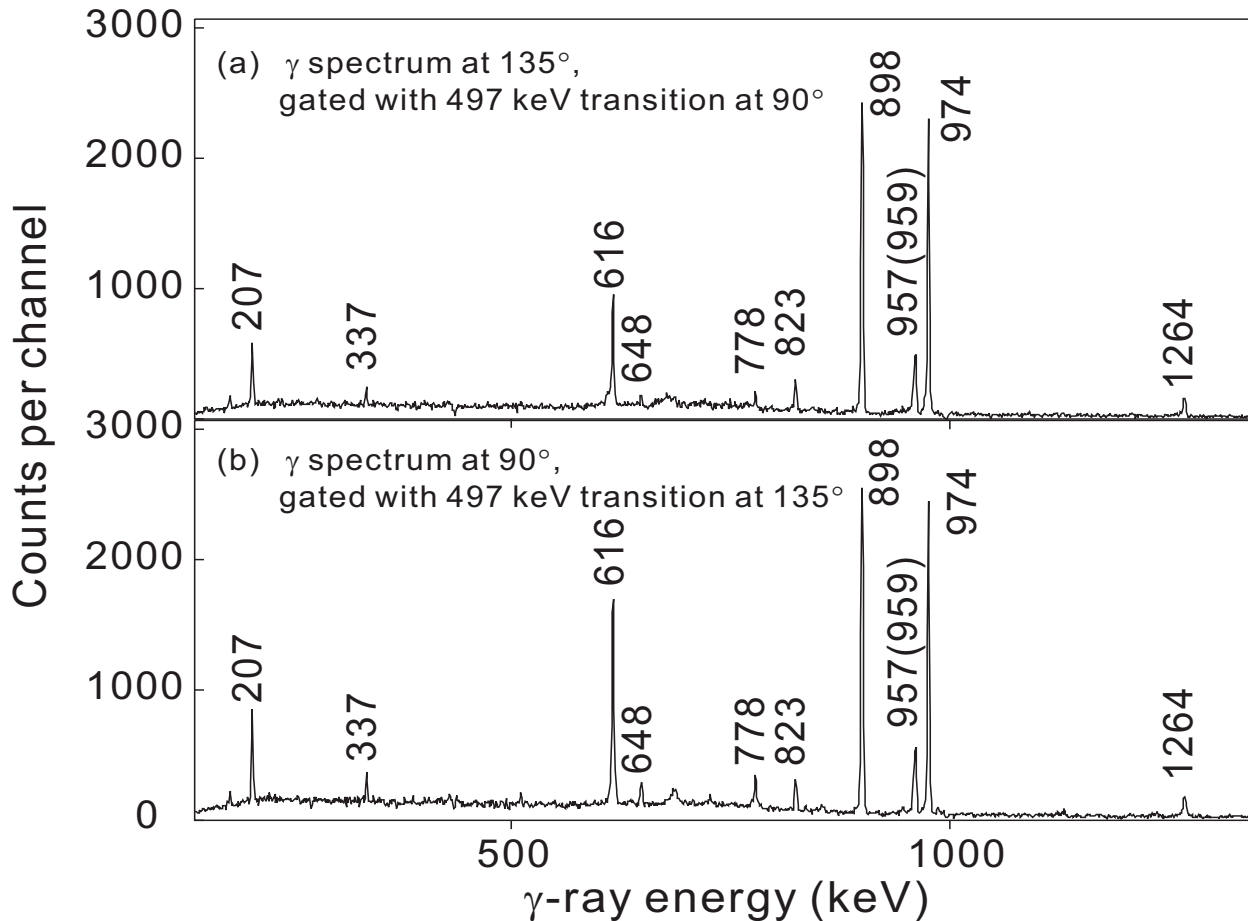


FIG. 2. (a) The projection of the DCO matrix on the  $135^\circ$  axis in coincidence with the 497 keV transition of  $^{91}\text{Ru}$  at  $90^\circ$ ; and (b) the projection on the  $90^\circ$  axis in coincidence with the same transition at  $135^\circ$ .

polarization of the  $\gamma$ -ray transitions (see below). For example, stretched  $E1$ ,  $E2$  or unstretched  $M1$  transitions and stretched  $M1$  or unstretched  $E1$  transitions have opposite sign linear polarization values [19].

In order to determine the multipolarity and the electromagnetic nature of a transition, both the DCO ratio and the linear polarization should be measured. One of the unique capabilities of the EXOGAM array is the possibility to use the clover detectors as Compton polarimeters. In the following, the measurement of the performances of EXOGAM as Compton polarimeter will be described. The clover detectors placed at  $90^\circ$  relative to the beam axis were used to determine the linear polarization of  $\gamma$ -ray transitions, since they are the most sensitive to the polarization [20]. We define the emission plane by the direction of the initial  $\gamma$ -ray and the beam axis. The clover detector is composed of four HPGe crystals closely packed in the same cryostat. In Compton scattering, the initial and scattered  $\gamma$ -rays can be detected in adjacent crystals of the same detector and analyzed separately according to whether the scattering has occurred horizontally to the emission plane or vertically to it.

Two  $\gamma$ - $\gamma$  matrices were created as follows: the first  $\gamma$ -ray corresponds to a single-crystal hit in any clover detector of the array and the second one to the sum of the energy deposited in two crystals within the same clover located at  $90^\circ$  (i.e. the addback energy of events scattering between two adjacent crystals of a clover, this one being positioned

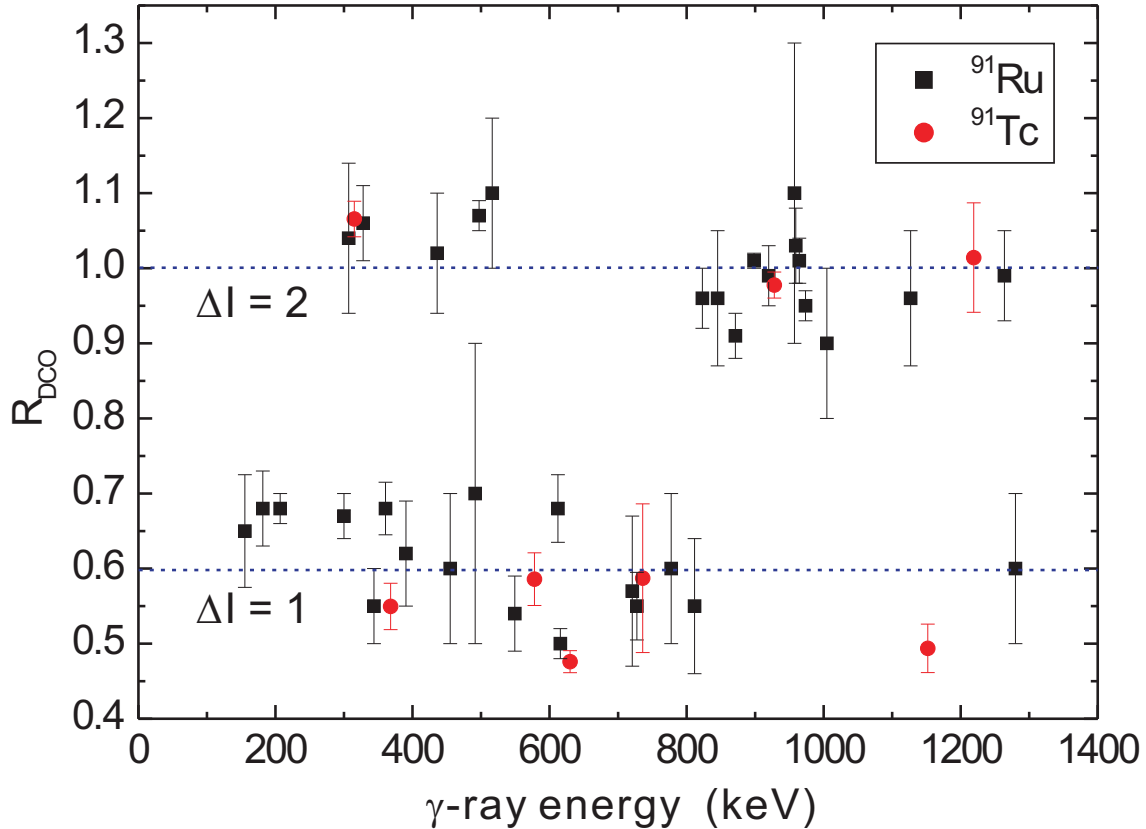


FIG. 3. (Color online) Experimental DCO ratios for the transitions belonging to  $^{91}\text{Ru}$  (■) and  $^{91}\text{Tc}$  (●). The lines correspond to the values obtained for known dipole and quadrupole transitions using gates on stretched quadrupoles and have been drawn to guide the eye.

at  $90^\circ$ ). The matrices contain therefore events with either horizontally or vertically scattered  $\gamma$ -rays in a clover at  $90^\circ$  on one axis and a single-crystal hit on any of the clover detectors on the other axis. The number of horizontal ( $N_\perp$ ) and vertical ( $N_\parallel$ ) scatters for a given  $\gamma$ -ray could be obtained by setting gates on  $\gamma$ -ray transitions in the two asymmetric matrices. The experimental polarization asymmetry is defined by the ratio  $A$ ,

$$A = \frac{[a(E_\gamma) N_\perp] - N_\parallel}{[a(E_\gamma) N_\perp] + N_\parallel}, \quad (2)$$

where  $a(E_\gamma)$  is the normalization factor corresponding to the asymmetry of the EXOGAM clover detectors, and is defined as

$$a(E_\gamma) = \frac{N_\parallel(\text{unpolarized})}{N_\perp(\text{unpolarized})}. \quad (3)$$

The normalization factor is a function of  $\gamma$ -ray energy and has been obtained from the measurement with a standard  $^{152}\text{Eu}$  radioactive source. Fig. 4 shows the variation of  $a$  with energy  $E_\gamma$ . It was fitted with the expression  $a(E_\gamma) = a_0 + a_1 E_\gamma$ , resulting in  $a_0 = 1.05(3)$  and  $a_1 = 3.9(9) \times 10^{-5}$ , where  $E_\gamma$  is in keV. As is clear from Fig. 4, the value of  $a$  is almost constant and close to unity, showing nearly ideal symmetry of the four-crystal clover detector acting as the Compton polarimeter.

The polarization asymmetry  $A$  is negative for unmixed stretched magnetic transitions and positive for stretched

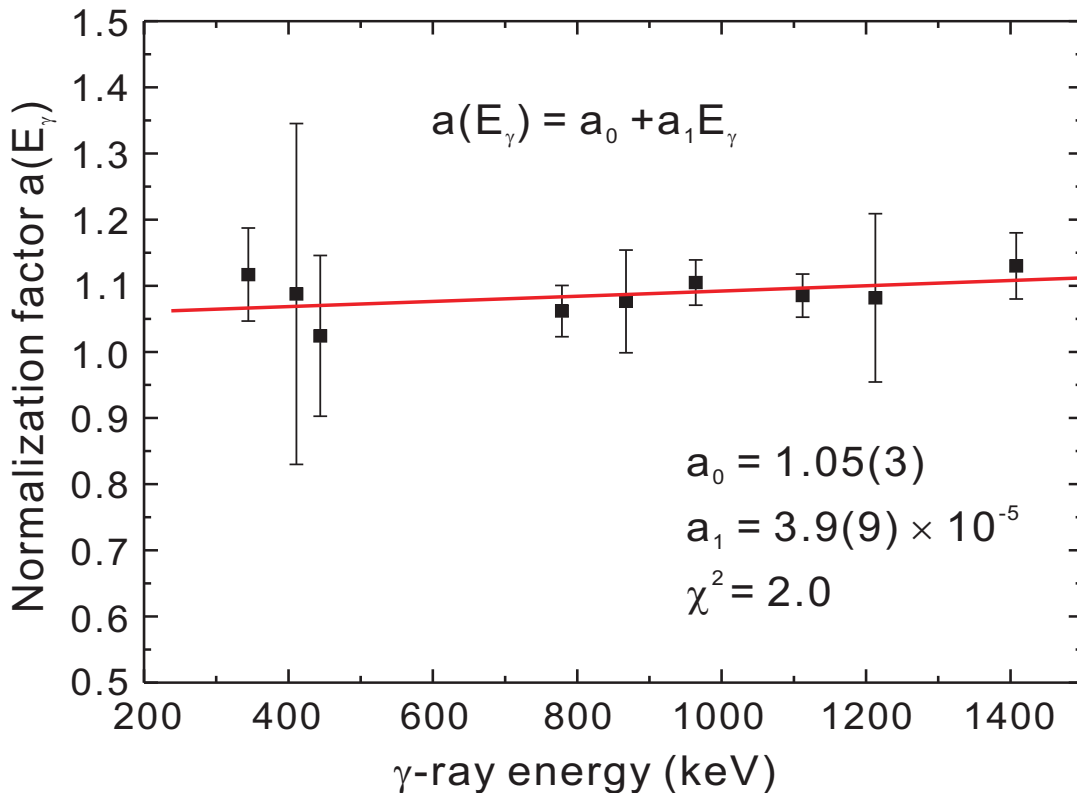


FIG. 4. (Color online) Normalization factor  $a$  in the linear polarization measurements as a function of  $\gamma$ -ray energy ( $E_\gamma$ ) for the EXOGAM array.

electric transitions. It is proportional to the degree of linear polarization  $P$ ,

$$A = QP, \quad (4)$$

where the quality factor  $Q$  is the polarization sensitivity of the polarimeter.  $Q = 0$  and  $Q = 1$  would indicate completely insensitive and completely sensitive polarimeters, respectively. For a point-like polarimeter, the polarization sensitivity  $Q$  can be calculated from the Klein-Nishina formula [21], which gives

$$Q_{\text{point}} = \frac{1 + \alpha}{1 + \alpha + \alpha^2} \quad \text{with} \quad \alpha = \frac{E_\gamma}{m_e c^2}, \quad (5)$$

where  $m_e$  is the electron rest mass. For a realistic setup of detectors with finite crystal size, we have to integrate over a certain range of scattering angles leading to a considerable reduction of the polarization sensitivity. The effective polarization sensitivity is usually given as

$$Q = Q_{\text{point}} \cdot (p_0 + p_1 E_\gamma) \quad (6)$$

According to eqs.(4)-(6),  $Q$  and the two parameters  $p_0$  and  $p_1$  can be experimentally determined using  $\gamma$ -rays whose linear polarization is well known. Theoretical values of the linear polarization can be deduced from the angular distribution. For  $\gamma$ -rays detected at  $90^\circ$  with respect to the beam direction, the polarization of pure electric quadrupole transitions can be calculated from the formula

$$P(90^\circ) = \frac{12A_2 + 5A_4}{8 - 4A_2 + 3A_4}, \quad (7)$$



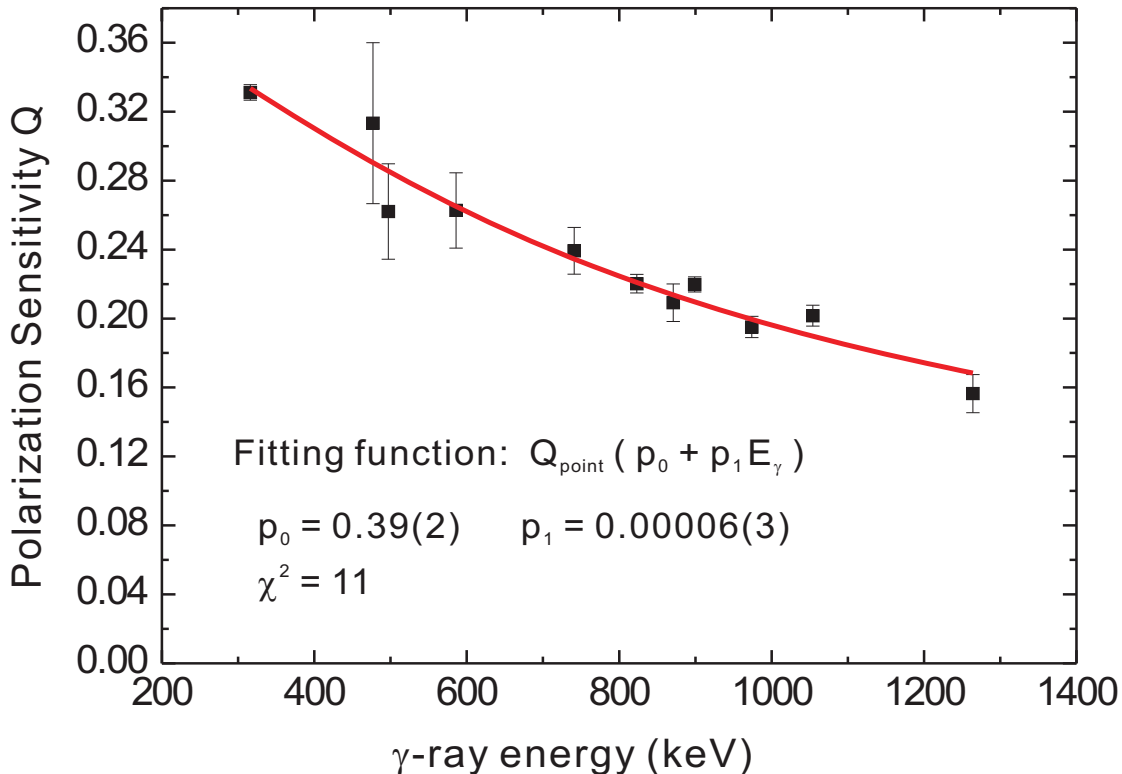


FIG. 5. (Color online) Polarization sensitivity of the EXOGAM detector. The solid line is the fit to our data.

where  $A_2$  and  $A_4$  are the normalized ( $A_0 = 1$ ) coefficients of the Legendre polynomials in the angular distribution.

To determine the capability of the EXOGAM array to measure linear polarization, we analyzed the angular distribution for the known pure  $E2$  transitions in the energy range 316 to 1264 keV in the level schemes of  $^{91}\text{Ru}$  [7],  $^{91}\text{Tc}$  [22],  $^{90}\text{Mo}$  [23], and  $^{88}\text{Mo}$  [24]. The angular distribution coefficients,  $A_2$  and  $A_4$ , for each transition, were extracted from least squares fits of the photopeak areas and summarized in Table I. The deduced values of the linear polarization  $P$  and the experimental asymmetry ratio  $A$  for the known  $\gamma$ -ray transitions are also summarized in Table I, along with the polarization sensitivity  $Q$  of the EXOGAM array. The experimental values of  $Q$ , together with the results of the fit to the data, are shown in Fig. 5. The coefficients  $p_0$  and  $p_1$  were determined by a least squares fit to the values of  $Q$  using the function of eq.(6);  $p_0 = 0.39 \pm 0.02$ ,  $p_1 = 0.00006 \pm 0.00003$ .

The quality of a polarimeter depends on both its sensitivity to the polarization and the coincidence efficiency between the scatterer and absorber crystals expressed as [25]

$$\epsilon_c(E_\gamma) = \frac{N_\perp + N_\parallel}{2N_{Clo}} \cdot \epsilon_{Clo}(E_\gamma), \quad (8)$$

where  $N_{Clo}$  and  $\epsilon_{Clo}$  are the total number of counts and the photopeak efficiency of the clover considered as a single detector at the energy  $E_\gamma$ , measured when the  $\gamma$ -ray has no polarization (i.e. using a source or when the detector is at  $0^\circ$  with respect to the beam direction). Finally it is common to compare polarimeters using a figure of merit defined as [25]

$$F = Q^2 \cdot \epsilon_c \quad (9)$$

The figure of merit deduced for the EXOGAM clover at 1368 keV is  $1.51 \times 10^{-5}$  which is 4.4 times larger than the one measured for the smaller EUROGAM clover [10]. At the same  $\gamma$ -ray energy, the measured polarization sensitivity  $Q_{\text{EXOGAM}}$  is 0.135(5) (0.121(5) for the EUROGAM clover) which means that the increase is due to the much larger coincidence efficiency. This increase in efficiency makes EXOGAM an ideal polarimeter for low-intensity  $\gamma$ -rays.

### III. RESULTS

The  $\gamma$ -rays from  $^{91}\text{Ru}$  were selected using the condition that two protons and one neutron were detected and with an additional selection on the two most intense transitions in  $^{91}\text{Ru}$ .  $\gamma$ -ray energies, intensity, DCO and asymmetry ratios have been measured (see Table II). Spins and parities of the levels have been assigned on the basis of the DCO ratios and the linear polarization results, respectively.

Fig. 6 illustrates a two dimensional plot of the asymmetry parameter  $A$  as a function of the DCO ratio when gating on a quadrupole transition. As can be seen from the plot, the polarization and multipolarity measurements together give us a reasonable assignment of the spin and parity for the levels.

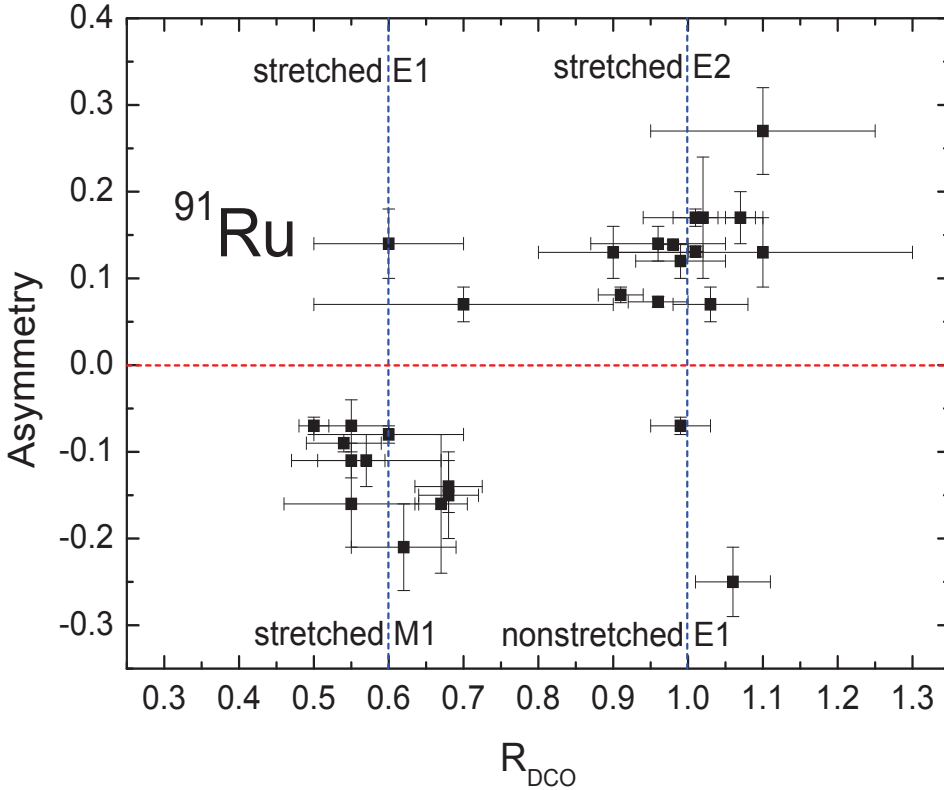


FIG. 6. (Color online) Two dimensional plot of the asymmetry ratio  $A$  as a function of the DCO ratio ( $R_{\text{DCO}}$ ) of the  $\gamma$ -rays belonging to  $^{91}\text{Ru}$ . Stretched  $E1$ ,  $E2$  and  $M1$  transitions and non-stretched  $E1$  transitions are indicated in the plot. The dashed lines parallel to the  $y$ -axis correspond to the value obtained for known pure stretched dipole and quadrupole transitions. These lines have been drawn to guide the eye. The  $R_{\text{DCO}}$  values have been obtained after gating on a quadrupole transition.

The deduced level scheme of  $^{91}\text{Ru}$  is shown in Fig. 7. States above spin  $(33/2)$  seen in [7] using the same reaction channel could not be observed in our data because of the lower beam energy (111 MeV compared to 149 MeV). The

analysis of our data revealed several new states. The ordering of the transitions in the level scheme are fixed either with the help of some crossover transitions or from the consideration of intensity balances in the gated spectra. The analysis of the low-level structure below the  $(13/2^-)$  state will be discussed in a forthcoming paper. In the present one, we focus on transitions indicated with a black asterisk in the level scheme of Fig. 7.

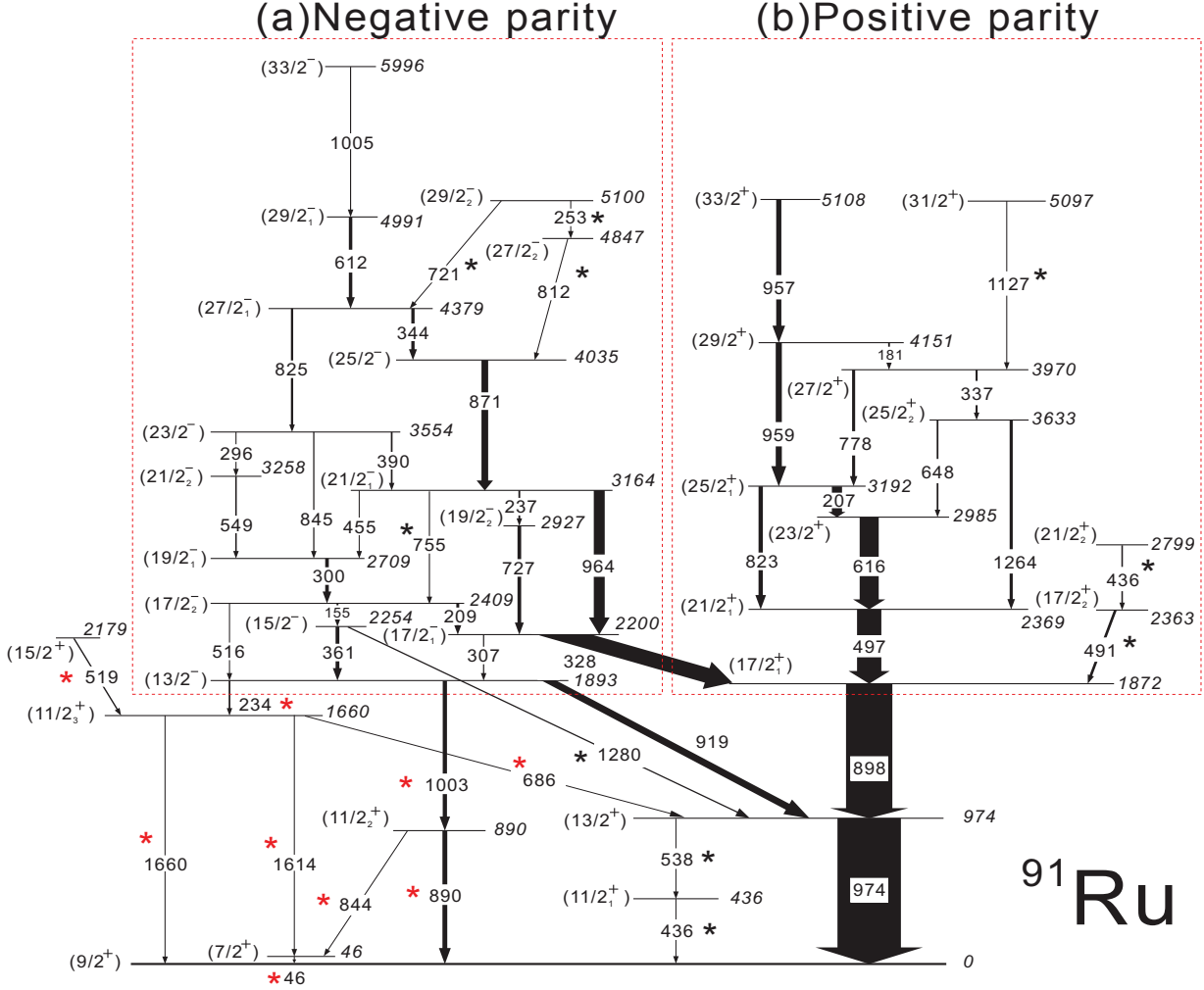


FIG. 7. (Color online) Level scheme of  $^{91}\text{Ru}$  proposed in the present work. The new transitions are indicated by asterisks. Those indicated with a red one will be discussed in a forthcoming paper.

In  $^{91}\text{Ru}$  the ground state has been assumed to be  $(9/2^+)$  [6–8]. This assumption is well supported by the decay study of  $^{91}\text{Ru}$  [26, 27] and the systematics of odd-A,  $N = 47$  isotones with  $36 \leq Z \leq 42$  [28]. Above the ground state, a strong transition sequence consisting of 974 keV, 898 keV, 497 keV, 823 keV, 959 keV, and 957 keV  $\gamma$ -rays was observed. The DCO ratio analysis indicates that they are quadrupole transitions. The polarization asymmetries for these quadrupole transitions are clearly positive, showing that they are stretched  $E2$  transitions and thus have been assigned as de-exciting the positive-parity levels as shown in the level scheme. A weak cascade of  $\gamma$ -rays with energies of 538 keV and 436 keV has been assigned to the present level scheme as parallel to the 974 keV,  $(13/2^+) \rightarrow (9/2^+)$  transition. The ordering of these two transitions is based on their relative intensities. In addition, the DCO ratio analysis and polarization measurement show that the weak 538 keV transition has a  $M1$  character, leading to the

assignment of  $(11/2^+)$  for the new yrast level at 436 keV. In the  $\beta$ -decay of  $^{91}\text{Rh}$  [9] several transitions were observed and assigned to feed the ground-state of  $^{91}\text{Ru}$ . Their placement in the level scheme is not confirmed in [8] but our measurement confirms the excited states at 436 keV and 890 keV. It is also noted that the 436 keV line is a doublet (see later).

Above the excited state at 974 keV, the level scheme is separated into two parts. One part is the group of positive-parity states which is on the right-hand side of the level scheme (Fig. 7(b)). The other part is the group of states on the left-hand side of the level scheme (Fig. 7(a)). Since no linear polarization measurement has been performed for this latter group of states up to now, the negative parity assignment proposed for those states in the earlier works [6, 7] could only be based on indirect evidence and hence was only tentative. Of primary importance in the linear polarization measurements are the most intense  $\gamma$ -ray transitions connecting the low-lying positive-parity states  $(17/2_1^+)$  and  $(13/2^+)$  of the yrast band and the presumed negative-parity levels. In  $^{91}\text{Ru}$  the key transitions for determining the parity of the left-side structure are the 328 keV, 919 keV and 1280 keV lines. From the results of the DCO ratio ( $\sim 1$  when gated by the stretched quadrupole transitions) and linear polarization measurements ( $A < 0$ ), a non-stretched  $\Delta I = 0$   $E1$  character (i.e. parity change) for the 328 keV and 919 keV connecting transitions is obtained. Thus these two  $\gamma$ -rays have been assigned as the  $(13/2^-) \rightarrow (13/2^+)$  and  $(17/2_1^-) \rightarrow (17/2_1^+)$  transitions, respectively. From the  $M1$  and  $E2$  character and multipolarity of the transitions depopulating levels above the  $(13/2^-)$  and  $(17/2_1^-)$  states lying at 1893 keV and 2200 keV respectively, negative parity has been assigned to these states. The DCO ratio and asymmetry measured for the 1280 keV transition are respectively 0.6(1) and 0.14(4) indicating an  $E1$  character, which is consistent with the previous assignments.

Up to the 5996 keV state, our spin assignments of the negative-parity level structure confirm the proposed values of Refs.[6, 7] but, from intensity considerations, the ordering of the 296 keV and 549 keV transitions is changed. The 549 keV transition in the sequence depopulates the 3258 keV state and feeds the  $J^\pi = (19/2_1^-)$ , 2709 keV state. This transition is a stretched magnetic dipole, and thus allows the assignment of  $J^\pi = (21/2_2^-)$  to the state at 3258 keV. The observation of the new  $\gamma$ -rays of 812 keV, 253 keV, and 721 keV lying above the  $(25/2^-)$  state at 4035 keV establishes two states as shown in Fig. 8. These two states, which are connected by the 253 keV transition, de-excite via the 812 keV and 721 keV  $\gamma$ -rays to the  $J^\pi = (25/2^-)$ , 4035 keV and  $J^\pi = (27/2_1^-)$ , 4379 keV states, respectively. The combination of the DCO ratio and linear polarization data determines the multiplicities of the 812 keV and 721 keV  $\gamma$ -rays to be both stretched  $M1$ . Therefore, spin and parity of  $(27/2_2^-)$  are assigned for the 4847 keV level and  $(29/2_2^-)$  for the 5100 keV level. This is further supported by the stretched dipole character of the 253 keV transition obtained from the DCO ratio analysis.

For the assignments of the positive-parity states, up to the  $(33/2^+)$  level at 5108 keV, our results are consistent with the earlier work of Refs.[6, 7]. In addition, three new transitions of 436 keV, 491 keV and 1127 keV have been observed below the  $(33/2^+)$  state. From the spectrum gated on the 436 keV peak shown in Fig. 1(c), the 436 keV transition is only in coincidence with the 491 keV line and the most intense 974 keV-898 keV transition sequence. The 538 keV line shown in this spectrum is in coincidence with the other 436 keV doublet transition and has been placed in the level scheme as feeding the new  $(11/2_1^+)$  state. Therefore, the 491 keV-436 keV cascade is proposed to be built directly on the  $(17/2_1^+)$  state at 1872 keV. The ordering of these two new transitions is determined from the relative intensities in the coincidence spectra. Based on the results of the DCO ratio and linear polarization measurements, the 491 and 436 keV  $\gamma$ -rays have been assigned as  $(17/2_2^+) \rightarrow (17/2_1^+)$  and  $(21/2_2^+) \rightarrow (17/2_1^+)$  transitions, respectively.

This results in the determination of the second  $(17/2_2^+)$  and  $(21/2_2^+)$  states at 2363 and 2799 keV, respectively. The weak 1127 keV transition populating the  $J^\pi = (27/2^+)$ , 3970 keV state shows a possible  $E2$  character; thus, the spin and parity of  $(31/2^+)$  is tentatively assigned to the 5097 keV state depopulated by the 1127 keV transition. We stress that except for this latter  $(31/2^+)$  state, it is *only* the ground state spin and parity uncertainty that needs resolving to allow all our assignments to be firmly established.

#### IV. SEMI-EMPIRICAL SHELL-MODEL CALCULATION AND DISCUSSION

To better understand the microscopic structure of the states of interest, a semi-empirical shell model was used. This allows the calculation of the excitation energy of complex multi-particle-hole configurations from the excitation energies of known configurations in neighboring nuclei. This method is parameter independent and was proposed by Garvey and Kelson [29, 30] for ground-state masses based on the prescription by Talmi and de Shalit [31, 32]. The technique was later extended by Blomqvist and collaborators [33] to calculate excited states in the  $A \sim 150$  and 200 mass regions. The approach restricts the analysis to states that predominantly contain a pure single-particle configuration as is expected for most of the yrast or near-yrast levels. We will mainly discuss the yrast and near-yrast seniority-three states. These level energies are calculated using nuclear ground-state masses, single-particle energies and two-particle interactions obtained from experimental data. The calculated results are compared with the experimental observations in Fig. 8 for the first and second  $(17/2^+)$  and  $(21/2^+)$  states. Input data for the calculations are taken from the neighbouring nuclei  $^{85,87,88}\text{Sr}$  [34, 35],  $^{87-90}\text{Zr}$  [36, 37],  $^{90-92}\text{Mo}$  [23, 38, 39], and  $^{93,94}\text{Ru}$  [40, 41]. Ground-state masses needed in the calculations are obtained from Ref. [42].

The non yrast states with  $J^\pi = (17/2_2^+)$  and  $(21/2_2^+)$  have been identified in  $^{91}\text{Ru}$  and added to the level scheme. As already mentioned previously, the simplest low-lying excitations expected for  $^{91}\text{Ru}$  are those arising from the  $\nu g_{9/2}^{-3}$  configuration terminating at spin  $21/2^+$ . However, as  $g_{9/2}$  protons are active, a different seniority scheme involving proton excitations, such as two  $g_{9/2}$  protons coupled to the unpaired  $g_{9/2}$  neutron hole, might become yrast in this nucleus. This  $\pi g_{9/2}^2 \nu g_{9/2}^{-1}$  multiplet terminates at spin  $25/2^+$ . In  $^{91}\text{Mo}$ , the three-quasiparticle seniority-three  $(\pi g_{9/2}^2 \nu g_{9/2}^{-1})21/2^+$  and  $17/2^+$  configurations were assigned to the 2268 and 2069 keV states, respectively [39]. Since the only active nucleons are  $g_{9/2}$  proton(s) and/or neutron(s), we will simplify the notation and omit the explicit reference to the  $g_{9/2}$  single-particle level. We will only specify the pairs that are coupled to  $0^+$  and the total angular momentum  $J_{Tot}$  when applicable i.e.:  $(\pi_{0^+}^i \pi^j \nu_{0^+}^k \nu^l) J_{Tot}$  means  $i$  protons in  $g_{9/2}$  coupled to  $0^+$ ,  $j$  protons in  $g_{9/2}$  *not* coupled to  $0^+$ , the same for the  $k$  and  $l$  neutrons, the total angular momentum being  $J_{Tot}$ . For instance the  $(\pi(g_{9/2})_{0^+}^2 (g_{9/2})^2 \nu(g_{9/2})_{0^+}^{-2} (g_{9/2})^{-1})21/2^+$  configuration will be reduced to  $(\pi_{0^+}^2 \pi^2 \nu_{0^+}^{-2} \nu^{-1})21/2^+$ .

The energies of the seven-quasiparticle seniority-three  $(\pi_{0^+}^2 \pi^2 \nu_{0^+}^{-2} \nu^{-1})21/2^+$  and  $17/2^+$  levels in  $^{91}\text{Ru}$  can be calculated from the above-mentioned  $\pi^2 \nu^{-1}$  states in  $^{91}\text{Mo}$  (see [18, 33] for the details). For example, with the known excitation energies of the concerned configurations in neighboring nuclei, the energy of the  $(\pi_{0^+}^2 \pi^2 \nu_{0^+}^{-2} \nu^{-1})21/2^+$  state is calculated as

$$E_{(\pi_{0^+}^2 \pi^2 \nu_{0^+}^{-2} \nu^{-1})21/2^+}^{91\text{Ru}} = E_{(\pi^2 \nu^{-1})21/2^+}^{91\text{Mo}} + \frac{23}{30} (E_{(\pi_{0^+}^2 \pi^2)8^+}^{94\text{Ru}} + E_{(\pi^2 \nu_{0^+}^{-2})8^+}^{90\text{Mo}} - 2E_{(\pi^2)8^+}^{92\text{Mo}})$$

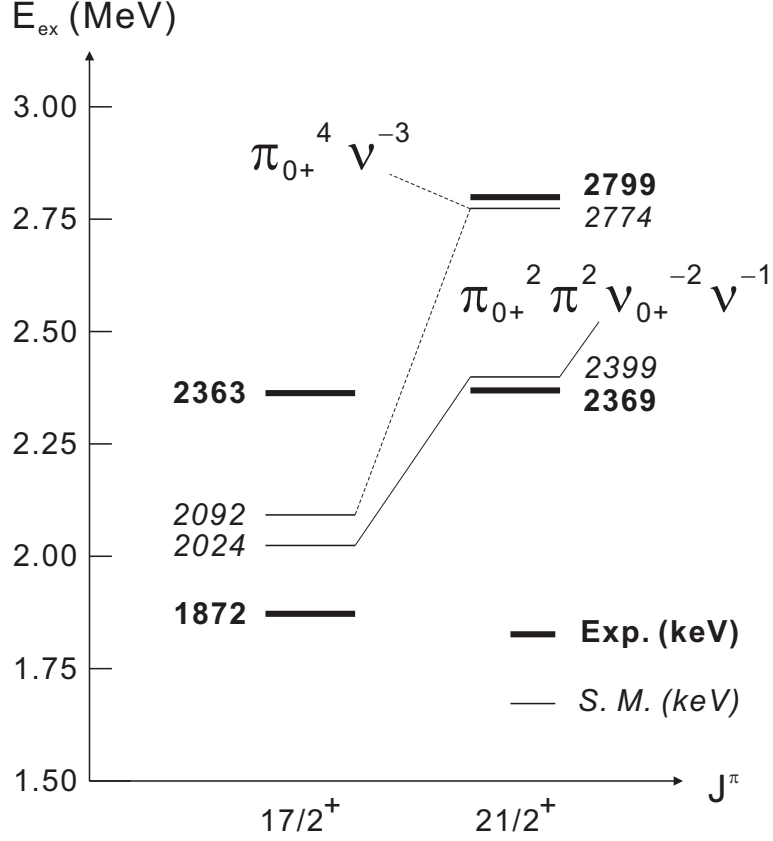


FIG. 8. Comparison between the calculated (thin lines) and experimentally observed (solid bars) ( $17/2^+$ ) and ( $21/2^+$ ) states in  $^{91}\text{Ru}$ . See text for the configuration notation.

$$\begin{aligned}
& + \frac{7}{30} (E_{(\pi_{0+}^2 \pi^2)6^+}^{94\text{Ru}} + E_{(\pi^2 \nu_{0+}^{-2})6^+}^{90\text{Mo}} - 2E_{(\pi^2)6^+}^{92\text{Mo}}) + S \\
& = 2399 \text{ keV}.
\end{aligned}$$

The fractions in the formula are angular momentum recoupling coefficients; in this reduction the mass term  $S$  is

$$\begin{aligned}
S & = 2M_{91\text{Mo}} + 2M_{90\text{Mo}} - 4M_{92\text{Mo}} + M_{87\text{Zr}} + 3M_{90\text{Zr}} - 2M_{88\text{Zr}} - 2M_{89\text{Zr}} + M_{94\text{Ru}} - M_{91\text{Ru}} \\
& = -99 \text{ keV}.
\end{aligned}$$

The energy of the  $17/2^+$  state with the same configuration is calculated in a similar way to be 2024 keV. The calculated energies of the seven-quasiparticle seniority-three ( $\pi_{0+}^2 \pi^2 \nu_{0+}^{-2} \nu^{-1}$ )  $21/2^+$  and  $17/2^+$  states are comparable to those of the yrast ( $21/2_1^+$ ) and ( $17/2_1^+$ ) levels observed at 2369 and 1872 keV, respectively, so we suggest that these levels have the dominant configuration of ( $\pi_{0+}^2 \pi^2 \nu_{0+}^{-2} \nu^{-1}$ ). This is consistent with the calculated results for these two levels in the previous work [7].

In  $^{85}\text{Sr}$  [34], the five-quasiparticle seniority-three ( $\pi_{0+}^{-2} \nu^{-3}$ )  $21/2^+$  and  $17/2^+$  configurations were identified at 3082 and 2400 keV. Therefore, the seven-quasiparticle seniority-three ( $\pi_{0+}^4 \nu^{-3}$ )  $21/2^+$  and  $17/2^+$  states might be expected in  $^{91}\text{Ru}$ . The excitation energy of the ( $\pi_{0+}^4 \nu^{-3}$ )  $21/2^+$  state is calculated to be

$$E_{(\pi_{0+}^4 \nu^{-3})}^{91\text{Ru}} = E_{(\pi_{0+}^{-2} \nu^{-3})21/2^+}^{85\text{Sr}} + 3E_{(\pi_{0+}^4 \nu^{-1})9/2^+}^{93\text{Ru}} - 3E_{(\pi_{0+}^{-2} \nu^{-1})9/2^+}^{87\text{Sr}} - 2E_{(\pi_{0+}^4)}^{94\text{Ru}} + S$$

$$= 2774 \text{ keV.}$$

In this case, the mass term  $S$  is

$$S = M_{s^5_{Sr}} - M_{91_{Ru}} + 3M_{93_{Ru}} - 3M_{s^7_{Sr}} + 2M_{s^8_{Sr}} - 2M_{94_{Ru}} = -308 \text{ keV.}$$

A similar calculation gives an energy of 2092 keV for the  $(\pi_{0+}^4 \nu^{-3})17/2^+$  configuration. The  $(21/2_2^+)$  and  $(17/2_2^+)$  levels are observed at 2799 and 2363 keV, and their energies are close to the calculated values of the  $(\pi_{0+}^4 \nu^{-3})21/2^+$  and  $17/2^+$  configurations. Therefore, the experimentally observed  $(21/2_2^+)$  and  $(17/2_2^+)$  states might be associated with the  $J_{\max}$  and  $J_{\max} - 2$  members of the seven-quasiparticle seniority-three  $(\pi_{0+}^4 \nu^{-3})$  multiplet. It is noted that these two states decay to the  $(17/2_1^+)$  state via the weak 491 keV  $\gamma$ -ray.

## V. SUMMARY

In the present work, we have used the EXOGAM Ge clover detectors as Compton polarimeters to measure the linear polarization of  $\gamma$ -ray transitions observed in  $^{91}\text{Ru}$ . The polarization sensitivity of the EXOGAM clover detectors has been obtained for incident  $\gamma$ -ray energies ranging from 300 to 1300 keV. Using the DCO ratios and linear polarization measurements, the nature and multipolarity of the transitions of interest have been deduced. However, since the ground state spin and parity in  $^{91}\text{Ru}$  is not yet measured, only the tentative spins and parities have been assigned to the yrast and non yrast states in  $^{91}\text{Ru}$ . We stress that resolving the ground state spin and parity would allow the firm assignment of all the identified levels except the  $(31/2^+)$  state. New  $(21/2_2^+)$  and  $(17/2_2^+)$  states have been observed at 430 keV and 491 keV above the yrast  $(21/2_1^+)$  and  $(17/2_1^+)$  states, respectively. Semi-empirical shell-model calculations have been done for these yrast and non yrast levels. The results clearly reveal the characteristic features of the active protons and neutrons in the  $g_{9/2}$  orbital. The  $(\pi_{0+}^2 \pi^2 \nu_{0+}^{-2} \nu^{-1})21/2^+$  and  $17/2^+$  configurations are proposed for the yrast  $(21/2^+)$  and  $(17/2^+)$  levels, and the  $(\pi_{0+}^4 \nu^{-3})21/2^+$  and  $17/2^+$  configurations are assigned to the non-yrast  $(21/2_2^+)$  and  $(17/2_2^+)$  levels.

## VI. ACKNOWLEDGMENT

The authors would like to thank the operators of the GANIL cyclotrons for providing the  $^{36}\text{Ar}$  beam. We would also like to thank the EXOGAM collaboration for use of the clover Ge detector array, the DIAMANT collaboration for use of the charged particle detector system, and the European  $\gamma$ -ray Spectroscopy Pool for use of the neutron detector system. We acknowledge funding support from the French-Polish LEA COPIGAL and the IN2P3-Polish laboratories COPIN agreement number 06-122, from the UK STFC, from the Swedish Research Council (contract nos 2007-4067 and 2008-5793), from the Göran Gustafsson Foundation, from the OTKA under contract number K100835 and from the Bolyai János Foundation. A. G. has been supported by the Generalitat Valenciana, Spain, under grant PROMETEO/2010/101 and by MINECO, Spain, under grants AIC-D-2011-0746 and FPA2011-29854. A. J acknowledge financial support from the Spanish Ministerio de Ciencia e Innovación under contract FPA2011-29854-

C04. Z. Y. acknowledges the support from the Chinese Academy of Sciences, China.

- 
- [1] E. Matthias, E. Recknagel, O. Hashimoto, S. Nagamiya, K. Nakai, T. Yamasaki, and Y. Yamasaki, *Nucl. Phys. A* **237**, 182 (1975).
- [2] O. Häusser, T. Faestermann, I. S. Towner, T. K. Alexander, H. R. Andrews, J. R. Beene, D. Horn, D. Ward, and C. Broude, *Hyperfine Interact.* **4**, 196 (1978).
- [3] M. Weiszflog, D. Rudolph, C. J. Gross, M. K. Kabadiyski, K. P. Lieb, H. Grawe, J. Heese, K. -H. Maier, J. Eberth, and S. Skoda, *Z. Phys. A* **344**, 395 (1993).
- [4] D. Zwarts, *Comp. Phys. Commun.* **38**, 365 (1985).
- [5] M. Weiszflog, A. Jungclaus, D. Kast, K. P. Lieb, R. Schubart, H. Grawe, J. Heese, and K. -H. Maier, *Z. Phys. A* **353**, 7 (1995).
- [6] S. E. Arnell, D. Foltescu, H. A. Roth, Ö. Skeppstedt, A. Nilsson, S. Mitarai, and J. Nyberg, *Phys. Scr.* **47**, 355 (1993).
- [7] J. Heese, H. Grawe, K. H. Maier, R. Schubart, F. Cristancho, C. J. Gross, A. Jungclaus, K. P. Lieb, D. Rudolph, J. Eberth, and S. Skoda, *Phys. Rev. C* **49**, 1896 (1994).
- [8] S. Dean, M. Górska, F. Aksouh, H. de Witte, M. Facina, M. Huyse, O. Ivanov, K. Krouglov, Yu. Kudryavtsev, I. Mukha, D. Smirnov, J.-C. Thomas, K. Van de Velc, J. Van de Walle, P. Van Duppen, and J. Van Roosbroeck, *Eur. Phys. J. A* **21**, 243 (2004).
- [9] M. Górska, S. Dean, V. Prasad N.V.S., A. Andreyev, B. Bruyneel, S. Franchoo, M. Huyse, K. Krouglov, R. Raabe, K. Van de Vel, P. Van Duppen, and J. Van Roosbroeck, *Proceedings of the International Workshop PINGST2000, Selected Topics on N=Z nuclei, June 2000, Lund, Sweden, Eds. D. Rudolph and M. Hellström, (Bloms i Lund AB, 2000).*
- [10] G. Duchêne, F.A. Beck, P.J. Twin, G. de France, D. Curien, L. Han, C.W. Beausang, M.A. Bentley, P.J. Nolan, J. Simpson, *Nucl. Instr. Meth. A* **432**, 90 (1999).
- [11] K. Andgren, E. Ganioglu, B. Cederwall, R. Wyss, S. Bhattacharyya, J. R. Brown, G. de Angelis, G. de France, Zs. Dombrádi, J. Gál, B. Hadinia, A. Johnson, F. Johnston-Theasby, A. Jungclaus, A. Khaplanov, J. Kownacki, K. Lagergren, G. La Rana, J. Molnár, R. Moro, B. S. Nara Singh, J. Nyberg, M. Sandzelius, J.-N. Scheurer, G. Sletten, D. Sohler, J. Timár, M. Trotta, J. J. Valiente-Dobón, E. Vardaci, R. Wadsworth, and S. Williams, *Phys. Rev. C* **76**, 014307 (2007).
- [12] J. Simpson, F. Azaiez, G. de France, J. Fouan, J. Gerl, R. Julin, W. Korten, P.J. Nolan, G. Sletten, P.M. Walker and the EXOGAM collaboration, *Acta Physica Hungarica, New Series, Heavy Ion Physics* **11**, 159 (2000).
- [13] Ö. Skeppstedt, H. A. Roth, L. Lindström, R. Wadsworth, I. Hibbert, N. Kelsall, D. Jenkins, H. Grawe, M. Górska, M. Moszyński, Z. Sujkowski, D. Wolski, M. Kapusta, M. Hellström, S. Kalogeropoulos, D. Oner, A. Johnson, J. Cederkäll, W. Klamra, J. Nyberg, M. Weiszflog, J. Kay, R. Griffiths, J. Garces Narro, C. Pearson, and J. Eberth, *Nucl. Instr. Meth. A* **421**, 531 (1999).
- [14] J. N. Scheurer, M. Aiche, M. M. Aléonard, G. Barreau, F. Bourguine, D. Boivin, D. Cabaussel, J. F. Chemin, T. P. Doan, J. P. Goudour, M. Harston, A. Brondi, G. La Rana, R. Moro, E. Vardaci, and D. Curien, *Nucl. Instr. Meth. A* **385**, 501 (1997).
- [15] J. Gál, G. Hegyesi, J. Molnár, B. M. Nyakó, G. Kalinka, J. N. Scheurer, M. M. Aléonard, J. F. Chemin, J. L. Pedroz, K. Juhász, and V. F. E. Pucknell, *Nucl. Instr. Meth. A* **516**, 502 (2004).
- [16] B. Cederwall, F. Ghazi Moradi, T. Bäck, A. Johnson, J. Blomqvist, E. Clément, G. de France, R. Wadsworth, K. Andgren, K. Lagergren, A. Dijon, G. Jaworski, R. Liotta, C. Qi, B.M. Nyakó, J. Nyberg, M. Palacz, H. Al-Azri, A. Algora, G. de Angelis, A. Atac, S. Bhattacharyya, T. Brock, J.R. Brown, P. Davies, A. Di Nitto, Zs. Dombradi, A. Gadea, J. Gál, B. Hadinia, F. Johnston-Theasby, P. Joshi, K. Juhász, R. Julin, A. Jungclaus, G. Kalinka, S.O. Kara, A. Khaplanov,



- J. Kownacki, G. La Rana, S.M. Lenzi, J. Molnár, R. Moro, D.R. Napoli, B.S. Nara Singh, A. Persson, F. Recchia, M. Sandzelius, J.-N. Scheurer, G. Sletten, D. Sohler, P.-A. Soderstrom, M.J. Taylor, J. Timar, J.J. Valiente-Dobon, E. Vardaci, and S. Williams, *Nature* **469**, 68 (2011).
- [17] K. S. Krane, R. M. Steffen, and R. M. Wheeler, *Nucl. Data Tables* **11**, 351 (1973).
- [18] M. Piiparinen, A. Ataç, J. Blomqvist, G. B. Hagemann, B. Herskind, R. Julin, S. Juutinen, A. Lampinen, J. Nyberg, G. Sletten, P. Tikkanen, S. Törmänen, A. Virtanen, R. Wyss, *Nucl. Phys. A* **605**, 191 (1996).
- [19] D. Sohler, I. Kuti, J. Timár, P. Joshi, J. Molnár, E. S. Paul, K. Starosta, R. Wadsworth, A. Algora, P. Bednarczyk, D. Curien, Zs. Dombrádi, G. Duchene, D. B. Fossan, J. Gál, A. Gizon, J. Gizon, D. G. Jenkins, K. Juhász, G. Kalinka, T. Koike, A. Krasznahorkay, B. M. Nyakó, P. M. Raddon, G. Rainovski, J. N. Scheurer, A. J. Simons, C. Vaman, A. R. Wilkinson, and L. Zolnai, *Phys. Rev. C* **85**, 044303 (2012).
- [20] B. Schlitt, U. Maier, H. Friedrichs, S. Albers, I. Bauske, P. von Brentano, R. D. Heil, R.-D. Merzberg, U. Kneissl, J. Margraf, H. M. Pitz, C. Wesselborg and A. Zilges, *Nucl. Instr. Meth. A* **337**, 416 (1994).
- [21] O. Klein, Y. Nishina, *Z. Phys.* **52**, 853 (1929).
- [22] D. Rudolph, C. J. Gross, A. Harder, M. K. Kabadiyski, K. P. Lieb, M. Weiszflog, J. Altmann, A. Dewald, J. Eberth, T. Mylaeus, H. Grawe, J. Heese, and K.-H. Maier, *Phys. Rev. C* **49**, 66 (1994).
- [23] P. Singh, R. G. Pillay, J. A. Sheikh, and H. G. Devare, *Phys. Rev. C* **45**, 2161 (1992).
- [24] M. Weiszflog, K. P. Lieb, F. Cristancho, C. J. Gross, A. Jungclaus, D. Rudolph, H. Grawe, J. Heese, K. -H. Maier, R. Schubart, J. Eberth, and S. Skoda, *Z. Phys. A* **342**, 257 (1992).
- [25] J. Simpson, P.A. Butler, L.P. Ekstrom, *Nucl. Instr. Meth. A* **204**, 463 (1983).
- [26] P. Komninos, E. Nolte, and P. Blasi, *Z. Phys.* **A314**, 135 (1983).
- [27] E. Hagberg, J. C. Hardy, H. Schmeing, E. T. H. Clifford, and V. T. Koslowsky, *Nucl. Phys. A* **395**, 152 (1983).
- [28] C. M. Lederer, V. S. Shirley, "Table of Isotopes, 7th Edition" (Wiley, New York 1978).
- [29] G. T. Garvey, T. Kelson, *Phys. Rev. Lett.* **16**, 197 (1966).
- [30] G. T. Garvey, *Annu. Rev. Nucl. Sci.* **19**, 433 (1969).
- [31] I. Talmi, *Rev. Mod. Phys.* **34**, 704 (1962).
- [32] A. de Shalit, I. Talmi, *Nuclear Shell Theory* (New York: Academic 1963).
- [33] J. Blomqvist, P. Kleinheinz, and P. J. Daly, *Z. Phys. A* **312**, 27 (1983).
- [34] S. E. Arnell, S. Sjöberg, Ö. Skeppstedt, and E. Wallander, *Nucl. Phys.* **A280**, 72 (1977).
- [35] L. P. Ekström, G. D. Jones, F. Kearns, T. P. Morrison, A. Nilsson, V. Paar, P. J. Twin, R. Wadsworth, E. Wallander, and N. J. Ward, *J. Phys. G: Nucl. Phys.* **7**, 85 (1981).
- [36] J. E. Kitching, P. A. Batay-Csorba, C. A. Fields, R. A. Ristinen, and B. L. Smith, *Nucl. Phys. A* **302**, 159 (1978).
- [37] J. Bendahan, C. Broude, E. Dafni, G. Goldring, M. Hass, E. Naim, and M. H. Rafailovich, *Phys. Rev. C* **33**, 1517 (1986).
- [38] M. K. Kabadiyski, F. Cristancho, C. J. Gross, A. Jungclaus, K. P. Lieb, D. Rudolph, H. Grawe, J. Heese, K. -H. Maier, J. Eberth, S. Skoda, W. -T. Chou, and E. K. Warburton, *Z. Phys. A* **343**, 165 (1992).
- [39] S. Ray, N. S. Pattabiraman, R. Goswami, S. S. Ghugre, A. K. Sinha, and U. Garg, *Phys. Rev. C* **69**, 054314 (2004).
- [40] P. Komninos, E. Nolte, *Z. Phys. A* **310**, 137 (1983).
- [41] W. J. Mills, J. J. Ressler, R. A. E. Austin, R. S. Chakrawarthy, D. S. Cross, A. Heinz, E. A. McCutchan, and M. D. Strange, *Phys. Rev. C* **75**, 047302 (2007).
- [42] The 2012 Update to the Atomic Mass Evaluation.

TABLE I.  $\gamma$ -ray energies, measured asymmetries, normalized angular distribution coefficients, deduced  $\gamma$ -ray polarization, and calculated polarization sensitivity of the EXOGAM clover Ge detectors. (Only known pure  $E2$  transitions have been used to determine the polarization sensitivity  $Q$ , see text.)

$E_\gamma$ (keV)	Channel	Nucleus	$J_i^\pi \rightarrow J_f^\pi$	Asymmetry	$A_2$	$A_4$	$P$	$Q$
316	3p	$^{91}\text{Tc}$	$21/2^+ \rightarrow 17/2^+$	0.17(2)	0.336(2)	-0.178(2)	0.513(2)	0.331(8)
477	4p	$^{90}\text{Mo}$	$12^+ \rightarrow 10^+$	0.16(4)	0.32(8)	-0.10(1)	0.51(9)	0.31(4)
497	2p1n	$^{91}\text{Ru}$	$21/2^+ \rightarrow 17/2^+$	0.17(3)	0.39(7)	-0.16(8)	0.65(8)	0.26(3)
586	2p1 $\alpha$	$^{88}\text{Mo}$	$8^+ \rightarrow 6^+$	0.11(3)	0.27(2)	-0.08(3)	0.42(4)	0.26(2)
741	2p1 $\alpha$	$^{88}\text{Mo}$	$2^+ \rightarrow 0^+$	0.068(7)	0.22(2)	-0.15(3)	0.28(5)	0.24(2)
823	2p1n	$^{91}\text{Ru}$	$25/2^+ \rightarrow 21/2^+$	0.073(6)	0.205(5)	-0.02(1)	0.33(1)	0.220(6)
871	2p1n	$^{91}\text{Ru}$	$25/2^- \rightarrow 21/2^-$	0.081(9)	0.23(3)	-0.01(1)	0.39(6)	0.21(1)
898	2p1n	$^{91}\text{Ru}$	$17/2^+ \rightarrow 13/2^+$	0.131(6)	0.33(1)	-0.01(2)	0.60(3)	0.220(4)
974	2p1n	$^{91}\text{Ru}$	$13/2^+ \rightarrow 9/2^+$	0.139(4)	0.39(3)	-0.02(5)	0.71(8)	0.195(6)
1054	4p	$^{90}\text{Mo}$	$4^+ \rightarrow 2^+$	0.114(5)	0.32(3)	-0.02(1)	0.57(6)	0.201(6)
1264	2p1n	$^{91}\text{Ru}$	$25/2^+ \rightarrow 21/2^+$	0.12(2)	0.41(4)	-0.01(1)	0.8(1)	0.16(1)

TABLE II. Properties of the  $\gamma$ -rays of  $^{91}\text{Ru}$ , produced in the  $^{58}\text{Ni}(^{36}\text{Ar}, 2p1n)^{91}\text{Ru}$  reaction. Uncertainties are given in parentheses. The gates used for the determination of the DCO ratios are indicated in the table.

$E_\gamma$ (keV) <sup>a</sup>	$I_\gamma$ (%) <sup>b</sup>	$E_i \rightarrow E_f$	$J_i^\pi \rightarrow J_f^\pi$	$R_{\text{DCO}}$	Gate <sub>DCO</sub> (keV)	Asymmetry
155.4	3.0(2)	2409 $\rightarrow$ 2254	(17/2 <sub>2</sub> <sup>-</sup> ) $\rightarrow$ (15/2 <sup>-</sup> )	0.65(7)	974	
181.6	2.7(1)	4151 $\rightarrow$ 3970	(29/2 <sup>+</sup> ) $\rightarrow$ (27/2 <sup>+</sup> )	0.68(5)	974	
206.9	16.0(4)	3192 $\rightarrow$ 2985	(25/2 <sub>1</sub> <sup>+</sup> ) $\rightarrow$ (23/2 <sup>+</sup> )	0.68(2)	497	
209.4	4.5(2)	2409 $\rightarrow$ 2200	(17/2 <sub>2</sub> <sup>-</sup> ) $\rightarrow$ (17/2 <sub>1</sub> <sup>-</sup> )			
236.8	2.9(3)	3164 $\rightarrow$ 2927	(21/2 <sub>1</sub> <sup>-</sup> ) $\rightarrow$ (19/2 <sub>2</sub> <sup>-</sup> )			
252.9	<0.6	5100 $\rightarrow$ 4847	(29/2 <sub>2</sub> <sup>-</sup> ) $\rightarrow$ (27/2 <sub>2</sub> <sup>-</sup> )			
296.0	1.6(2)	3554 $\rightarrow$ 3258	(23/2 <sup>-</sup> ) $\rightarrow$ (21/2 <sub>2</sub> <sup>-</sup> )			
299.9	5.6(2)	2709 $\rightarrow$ 2409	(19/2 <sub>1</sub> <sup>-</sup> ) $\rightarrow$ (17/2 <sub>2</sub> <sup>-</sup> )	0.67(3)	974	-0.16(8)
306.8	1.9(2)	2200 $\rightarrow$ 1893	(17/2 <sub>1</sub> <sup>-</sup> ) $\rightarrow$ (13/2 <sup>-</sup> )	1.04(10)	974	
328.0	25.1(1)	2200 $\rightarrow$ 1872	(17/2 <sub>1</sub> <sup>-</sup> ) $\rightarrow$ (17/2 <sub>1</sub> <sup>+</sup> )	1.06(5)	898	-0.25(4)
336.5	3.2(2)	3970 $\rightarrow$ 3633	(27/2 <sup>+</sup> ) $\rightarrow$ (25/2 <sub>2</sub> <sup>+</sup> )			
343.8	5.2(1)	4379 $\rightarrow$ 4035	(27/2 <sup>-</sup> ) $\rightarrow$ (25/2 <sup>-</sup> )	0.55(5)	974	-0.07(3)
360.6	5.9(2)	2254 $\rightarrow$ 1893	(15/2 <sup>-</sup> ) $\rightarrow$ (13/2 <sup>-</sup> )	0.68(4)	974	-0.15(5)
390.5	2.7(2)	3554 $\rightarrow$ 3164	(23/2 <sup>-</sup> ) $\rightarrow$ (21/2 <sub>1</sub> <sup>-</sup> )	0.62(7)	974	-0.21(5)
435.9	2.4(2)	2799 $\rightarrow$ 2363	(21/2 <sub>2</sub> <sup>+</sup> ) $\rightarrow$ (17/2 <sub>2</sub> <sup>+</sup> )	1.02(8)	974	0.17(7)
436.0	<0.4	436 $\rightarrow$ 0	(11/2 <sub>1</sub> <sup>+</sup> ) $\rightarrow$ (9/2 <sup>+</sup> )			
455.0	1.0(1)	3164 $\rightarrow$ 2709	(21/2 <sub>1</sub> <sup>-</sup> ) $\rightarrow$ (19/2 <sub>1</sub> <sup>-</sup> )	0.6(1)	974	
491.4	4.2(2)	2363 $\rightarrow$ 1872	(17/2 <sub>2</sub> <sup>+</sup> ) $\rightarrow$ (17/2 <sub>1</sub> <sup>+</sup> )	0.7(2)	974	0.07(2)
497.2	38.3(1)	2369 $\rightarrow$ 1872	(21/2 <sub>1</sub> <sup>+</sup> ) $\rightarrow$ (17/2 <sub>1</sub> <sup>+</sup> )	1.07(2)	974	0.17(3)
516.4	1.1(1)	2409 $\rightarrow$ 1893	(17/2 <sub>2</sub> <sup>-</sup> ) $\rightarrow$ (13/2 <sup>-</sup> )	1.1(1)	974	0.27(5)
538.0	<0.4	974 $\rightarrow$ 436	(13/2 <sup>+</sup> ) $\rightarrow$ (11/2 <sub>1</sub> <sup>+</sup> )	1.1(6)	361	-0.19(8)
549.3	2.4(2)	3258 $\rightarrow$ 2709	(21/2 <sub>2</sub> <sup>-</sup> ) $\rightarrow$ (19/2 <sub>1</sub> <sup>-</sup> )	0.54(5)	974	-0.09(1)
612.3	5.4(2)	4991 $\rightarrow$ 4379	(29/2 <sup>-</sup> ) $\rightarrow$ (27/2 <sup>-</sup> )	0.68(4)	871	-0.14(3)
615.8	30.0(5)	2985 $\rightarrow$ 2369	(23/2 <sup>+</sup> ) $\rightarrow$ (21/2 <sub>1</sub> <sup>+</sup> )	0.50(2)	497	-0.07(1)
648.0	2.8(2)	3633 $\rightarrow$ 2985	(25/2 <sub>2</sub> <sup>+</sup> ) $\rightarrow$ (23/2 <sup>+</sup> )			
720.7	0.7(1)	5100 $\rightarrow$ 4379	(29/2 <sub>2</sub> <sup>-</sup> ) $\rightarrow$ (27/2 <sup>-</sup> )	0.57(10)	871	-0.11(3)
727.5	5.8(3)	2927 $\rightarrow$ 2200	(19/2 <sub>2</sub> <sup>-</sup> ) $\rightarrow$ (17/2 <sub>1</sub> <sup>-</sup> )	0.55(4)	974	-0.11(2)
754.5	1.7(2)	3164 $\rightarrow$ 2409	(21/2 <sub>1</sub> <sup>-</sup> ) $\rightarrow$ (17/2 <sub>2</sub> <sup>-</sup> )			
777.5	4.8(1)	3970 $\rightarrow$ 3192	(27/2 <sup>+</sup> ) $\rightarrow$ (25/2 <sub>1</sub> <sup>+</sup> )	0.6(1)	974	-0.08(1)
811.6	0.8(1)	4847 $\rightarrow$ 4035	(27/2 <sub>2</sub> <sup>-</sup> ) $\rightarrow$ (25/2 <sup>-</sup> )	0.55(9)	871	-0.16(5)
823.0	6.8(2)	3192 $\rightarrow$ 2369	(25/2 <sub>1</sub> <sup>+</sup> ) $\rightarrow$ (21/2 <sub>1</sub> <sup>+</sup> )	0.96(4)	497	0.073(6)
824.7	3.6(2)	4379 $\rightarrow$ 3554	(27/2 <sup>-</sup> ) $\rightarrow$ (23/2 <sup>-</sup> )			
845.3	2.0(1)	3554 $\rightarrow$ 2709	(23/2 <sup>-</sup> ) $\rightarrow$ (19/2 <sub>1</sub> <sup>-</sup> )	0.96(9)	974	0.14(2)
871.2	10.5(1)	4035 $\rightarrow$ 3164	(25/2 <sup>-</sup> ) $\rightarrow$ (21/2 <sub>1</sub> <sup>-</sup> )	0.91(3)	974	0.081(9)
898.5	73(1)	1872 $\rightarrow$ 974	(17/2 <sub>1</sub> <sup>+</sup> ) $\rightarrow$ (13/2 <sup>+</sup> )	1.01(1)	974	0.131(6)
919.8	11.3(1)	1893 $\rightarrow$ 974	(13/2 <sup>-</sup> ) $\rightarrow$ (13/2 <sup>+</sup> )	0.99(4)	974	-0.07(1)
957.4	8.1(3)	5108 $\rightarrow$ 4151	(33/2 <sup>+</sup> ) $\rightarrow$ (29/2 <sup>+</sup> )	1.1(2)	1264	0.13(4)
959.4	9.6(3)	4151 $\rightarrow$ 3192	(29/2 <sup>+</sup> ) $\rightarrow$ (25/2 <sub>1</sub> <sup>+</sup> )	1.03(5)	957	0.07(2)
964.5	17.3(3)	3164 $\rightarrow$ 2200	(21/2 <sub>1</sub> <sup>-</sup> ) $\rightarrow$ (17/2 <sub>1</sub> <sup>-</sup> )	1.01(3)	871	0.17(1)
973.5	100	974 $\rightarrow$ 0	(13/2 <sup>+</sup> ) $\rightarrow$ (9/2 <sup>+</sup> )	0.95(2)	497	0.139(4)
1004.7	1.7(1)	5996 $\rightarrow$ 4991	(33/2 <sup>-</sup> ) $\rightarrow$ (29/2 <sup>-</sup> )	0.9(1)	974	0.13(3)
1126.9	0.8(1)	5097 $\rightarrow$ 3970	(31/2 <sup>+</sup> ) $\rightarrow$ (27/2 <sup>+</sup> )	0.96(9)	497	
1263.9	4.9(2)	3633 $\rightarrow$ 2369	(25/2 <sub>2</sub> <sup>+</sup> ) $\rightarrow$ (21/2 <sub>1</sub> <sup>+</sup> )	0.99(6)	974	0.12(2)
1280.7	2.1(8)	2254 $\rightarrow$ 974	(15/2 <sup>-</sup> ) $\rightarrow$ (13/2 <sup>+</sup> )	0.6(1)	974	0.14(4)

<sup>a</sup> Energy uncertainties are within 0.5 keV.

<sup>b</sup>  $\gamma$ -ray intensities relative to the (13/2<sup>+</sup>)  $\rightarrow$  (9/2<sup>+</sup>) 974 keV transition.